Numerical simulations

LOTHAR BANZ[1], ADRIAN COSTEA[1], HEIKO GIMPERLEIN AND ERNST P. STEPHAN[1*]

1 Institut für Angewandte Mathematik, Leibniz Universität Hannover, Welfengarten 1, 30167 Hannover, Germany (banz@ifam.uni-hannover.de, costea@ifam.uni-hannover.de, stephan@ifam.uni-hannover.de)

2 Department of Mathematical Sciences, University of Copenhagen, Universitetsparken 5, 2100 Copenhagen, Denmark (gimperlein@math.ku.dk)

* Corresponding author

Received: July 11, 2013; Revised: November 15, 2013; Accepted: January 14, 2014

ABSTRACT

We present a boundary element method to compute numerical approximations to the non-linear Molodensky problem, which reconstructs the surface of the Earth from the gravitational potential and the gravity vector. Our solution procedure solves a sequence of exterior oblique Robin problems and is based on a Nash-Hörmander iteration. We apply smoothing with the heat equation to overcome a loss of derivatives in the surface update. Numerical results show the error between the approximation and the exact solution in a model problem.

Keywords: Molodensky problem, Nash-Hörmander iteration, heat-kernel smoothing, boundary elements

1. INTRODUCTION

The determination of the shape of the Earth and its exterior gravitational field from terrestrial measurements is a basic problem in physical geodesy (*Beck, 2002*; *Heiskanen and Moritz, 1993*). *Molodensky (1958, 1960)* formulated it as an exterior free boundary problem for the Laplace equation in $\mathbb{R}^3$ with the gravity potential W and field G prescribed on an unknown boundary diffeomorphic to the two-dimensional sphere $\mathbb{S}$ by a map $\varphi : \mathbb{S}^2 \to \mathbb{R}^3$. With the advent of satellite technologies to determine the surface of the Earth high-precision studies combine satellite data with local gravity measurements.

Hörmander (1976) proved local existence and uniqueness of the solution of Molodensky's problem. Based on ideas of *Nash (1960)* and *Moser (1966a,b)*, his constructive proof overcomes the loss of regularity of subsequent iterates in standard fixed-point methods for this problem by introducing an additional smoothing operator in each step. In *Costea et al. (2013)* we have shown that smoothing by a higher-order heat equation can be used and is numerical feasible. We have obtained error estimates for the iterates showing the dependence of the rate of convergence of the algorithm on certain parameters.

Here we present some computational aspects of our approach to the non-linear Molodensky problem. To solve the free boundary problem we iteratively construct a sequence $(\varphi_m)_{m\in\mathbb{N}_0}$ of approximations to the boundary φ, where φ_m is obtained from the boundary element solution of the problem linearized around φ_{m-1}. The numerical solution of the linearized Molodensky problem using the boundary element method with piecewise linear ansatz functions was first analyzed by *Klees et al. (2001)*, see also *Holota (1997)*, *Freeden and Mayer (2006)*, *Čunderlík et al. (2008)* and *Čunderlík and Mikula (2010)*. Smoothed iterative solvers involving the heat equation were investigated in *Jerome (1985)* and *Fasshauer and Jerome (1990)* for ordinary differential equations.

In Section 2 we present the Nash-Hörmander algorithm and in Section 3 the boundary element procedure. Section 4 gives the detailed description for a model problem in which the sphere of radius 1.1 is recovered by our method starting from the unit sphere.

However, our solution procedure should be applicable to more complicated geometries like spheroids, telluroids, etc. The theoretical analysis of the here given procedure from *Costea et al. (2013)* ensures convergence when discretization errors, mainly due to surface approximation, are neglected. These errors accumulate in the iterations. An application to realistic geodetic data would require further study of higher order surface approximation and restarted versions of the algorithm. In particular, to be relevant for the geodetic community, one might model the exact surface by the ETOPO1 model of the Earth and compute the gravity vector from the EGM2008 model. A more realistic model problem could then try to recover φ starting from the GRS80 ellipsoid as surface φ_0 and the corresponding Somigliani-Pizzetti field as (W_0, G_0) (*Ardalan and Grafarend, 2001*).

2. THE NASH-HÖRMANDER ALGORITHM

A classical problem in geodesy is to find an embedding $\varphi:\mathbb{S}^2\to\mathbb{R}^3$ such that $G=\Gamma(W,\varphi)$ where the potential W and the gravity vector G are given on $\mathbb{S}^2$. We assume that the Earth is a rigid body rotating with a constant angular velocity ω around a fixed axes, which we choose as the x_3 axis. The nonlinear map Γ is implicitly described by the nonlinear Molodensky problem (Eqs (1)): Find $\varphi:\mathbb{S}^2\to\mathbb{R}^3$ subject to

$$\begin{aligned} &\Delta v = 0 \quad \text{outside} \quad \varphi\left(\mathbb{S}^2\right), \\ &w = W\circ\varphi^{-1}, \quad g := G\circ\varphi^{-1} \quad \text{on} \quad \varphi\left(\mathbb{S}^2\right), \\ &v(x) = \frac{M}{|x|} + O\left(|x|^{-3}\right) \quad \text{when} \quad |x|\to\infty, \quad M\in\mathbb{R}, \end{aligned} \tag{1}$$

where $w=(1/2)\omega^2\left(x_1^2+x_2^2\right)+v$ with the gravitational potential v and symbol $\circ$ denotes the composition. In this model the decay condition fixes the center of mass of the Earth $\varphi\left(\mathbb{S}^2\right)$ at the origin.

In *Hörmander (1976)*, the nonlinear Molodensky problem (Eq. (1)) is solved by a sequence of linearized problems together with a specific smoothing of a Newton-like iteration. Hörmander shows convergence of his sequence of approximate solutions. A rate of convergence of the iteration was derived in *Costea et al. (2013)*, where a boundary element procedure was suggested to solve Eq. (1). Here we present numerical experiments with the solution procedure from *Costea et al. (2013)* and describe how to apply the heat equation as a smoother within this context. In each step of the iteration one solves a linearized Molodensky problem (2) for a given right hand side F depending on the current solution sequence (as given explicitly below in Eqs (3)): Find u and $a_j \in \mathbb{R}$ such that

$$\begin{aligned} &\Delta v = 0 \quad \text{outside} \quad \varphi\left(\mathbb{S}^2\right), \\ &u + \nabla u \cdot h = F\left(G, W\right) - \sum_{j=1}^{3} a_j A_j \quad \text{on} \quad \varphi\left(\mathbb{S}^2\right), \\ &u(x) = \frac{c}{|x|} + O\left(|x|^{-3}\right) \quad \text{when} \quad |x| \to \infty, \quad c \in \mathbb{R}, \end{aligned} \tag{2}$$

where the Marussi condition $\det\left(\nabla g\right) \neq 0$ on $\varphi\left(S^2\right)$ for $g = \nabla U$ with a fixed U is assumed to hold. The vector h in Eq. (2) satisfies $h = -\left(\nabla g\right)^{-1} g$. The functions $A_j = x_j \big/ |x|^3$ guarantee that Eq. (2) is well-posed under certain conditions, see *Hörmander (1976)* and *Costea et al. (2013)*.

Then one updates φ by the increment $\Delta\dot{\varphi} = \Delta\left(\nabla g \circ \varphi\right)^{-1}\left(\dot{G} - \nabla u \circ \varphi\right)$, where $\dot{G}$ is the increment of $\boldsymbol{G}$. One observes as main difficulty in constructing φ that $\dot{\varphi}$ is less regular than φ. We overcome this dilemma by applying the heat-equation as described below obtaining the smoothed quantities $\dot{\widetilde{W}}_m$ and $\dot{\widetilde{G}}_m$. The Nash-Hörmander iteration for Eq. (1) reads as follows: At each iteration step, for $F_m = \dot{\widetilde{W}}_m \circ \varphi_m^{-1} + \left(\dot{\widetilde{G}}_m \circ \varphi_m^{-1}\right) \cdot h_m$ (as specified below) find u_m and $a_{j,m} \in \mathbb{R}$ such that

$$\begin{aligned} &\Delta u_m = 0 \quad \text{outside} \quad \varphi_m\left(\mathbb{S}^2\right), \\ &u_m + \nabla u_m \cdot h_m = F_m - \sum_{j=1}^{3} a_{j,m} A_j \quad \text{on} \quad \varphi_m\left(\mathbb{S}^2\right), \\ &u_m(x) = \frac{c}{|x|} + O\left(|x|^{-3}\right) \quad \text{when} \quad |x| \to \infty, \quad c \in \mathbb{R}, \end{aligned} \tag{3}$$

with $\det\left(\nabla g_{m-1}\right) \neq 0$ on $\varphi_m\left(S^2\right)$ and

$$g_{m-1} = \nabla\left[w_{m-1} + \frac{1}{2}\omega^2\left(x_1^2 + x_2^2\right)\right] = \nabla\left[\sum_{j=0}^{m-1} u_j + \frac{1}{2}\omega^2\left(x_1^2 + x_2^2\right)\right]$$

and

$$h_m = \left[-\left(\nabla g_{m-1}\right)^{-1} g_{m-1} \circ \varphi_{m-1} \right] \circ \varphi_m^{-1}, \quad A_j = \frac{x_j}{|x|^3}.$$

The solution u_m determines the nonlinear correction $\dot{\varphi}_m$, i.e. $\varphi_{m+1} = \varphi_m + \delta_m \dot{\varphi}_m$, namely

$$\dot{\varphi}_m = \left(\nabla g_m \circ \varphi_m\right)^{-1}\left(\dot{\tilde{G}}_m - \nabla u_m \circ \varphi_m \right). \tag{4}$$

The vector g_m is determined from the approximation to the potential as computed in the first *m* steps,

$$\begin{aligned} w_m &= W_{m-1} \circ \varphi_m^{-1} + \Delta_m u_m \quad \text{on} \quad \varphi_m\left(S^2\right), \\ W_{m-1} &= \begin{cases} v_0 \circ \varphi_0 + \Delta_0 u_0 \circ \varphi_0 + \Delta_1 u_1 \circ \varphi_1 + \ldots + \Delta_{m-1} u_{m-1} \circ \varphi_{m-1} & \text{for} \quad m \geq 1, \\ v_0 \circ \varphi_0 \quad \text{for} \quad m = 0, \end{cases} \end{aligned} \tag{5}$$

for suitable stepsizes Δ_j and initial approximation v_0 by solving an exterior Dirichlet problem: For given w_m on $\varphi_m\left(S^2\right)$, find $\overline{v}_m : \mathbb{R}^3 \setminus \overline{\Omega}_m \to \mathbb{R}$ and constants $a_{j,m} \in \mathbb{R}$ such that

$$\begin{aligned} \Delta \overline{v}_m &= 0 \quad \text{in} \quad \mathbb{R}^3 \setminus \overline{\Omega}_m, \\ \overline{v}_{m|_{\partial\Omega_m}} &= w_m - \sum_{j=1}^{3} a_{j,m} A_j\left(x\right)\Big|_{x \in \varphi_m\left(S^2\right)} \quad \text{on} \quad \varphi_m\left(S^2\right), \\ \overline{v}_m\left(x\right) &= \frac{c}{|x|} + O\left(|x|^{-3}\right) \quad \text{when} \quad |x| \to \infty. \end{aligned} \tag{6}$$

Now with Eq. (4) the surface update $\dot{\varphi}_m$ is computed using $g_m = \nabla\left[\overline{v}_m + (1/2)\omega^2\left(x_1^2 + x_2^2\right)\right]$ and $\nabla g_m = \nabla^2\left[\overline{v}_m + (1/2)\omega^2\left(x_1^2 + x_2^2\right)\right]$.

The full iterative method involves smoothing in each step based on the solution operator S_θ to a higher-order heat equation (discussed below). It reads as follows:

Algorithm 1. (Nash-Hörmander algorithm)

1. For given measured data W, G, choose W_0, G_0, h_0, φ_0, $\kappa \gg 1$ and smoother S_θ
2. For $m = 0, 1, 2, \ldots$ do
   a) Compute

$$\theta_m = \left(\theta_0^\kappa + m\right)^{1/\kappa}, \quad \Delta_m = \theta_{m+1} - \theta_m \tag{7}$$

   b) Compute

$$\begin{aligned} \dot{\widetilde{W}}_0 &:= S_{\theta_0} \dot{W}_0 = S_{\theta_0} \frac{W - W_0}{\Delta_0}, \\ \dot{\widetilde{W}}_m &:= \frac{1}{\Delta_m}\left[S_{\theta_0}\left(W - W_0\right) - S_{\theta_{m-1}}\left(W - W_0\right)\right] \end{aligned} \tag{8}$$

   c) Compute

$$\begin{aligned} \dot{\widetilde{G}}_0 &:= S_{\theta_0} \dot{G}_0 = S_{\theta_0} \frac{G - G_0}{\Delta_0}, \\ \dot{\widetilde{G}}_m &:= \frac{1}{\Delta_m}\left[S_{\theta_0}\left(G - G_m + \sum_{j=0}^{m-1} \Delta_j \dot{\widetilde{G}}_j \right) - S_{\theta_{m-1}}\left(G - G_{m-1} + \sum_{j=0}^{m-2} \Delta_j \dot{\widetilde{G}}_j \right)\right] \end{aligned} \tag{9}$$

   d) Find u_m by solving the linearized problem given by Eqs (3) with $\left(\dot{W}_m, \dot{G}_m\right)$ replaced by $\left(\dot{\widetilde{W}}_m, \dot{\widetilde{G}}_m\right)$

   e) Find $\overline{v}_m$ by solving Eq. (6) with w_m as defined in Eq. (5)

   f) Compute

$$g_m = \nabla\left[\overline{v}_m + (1/2)\omega^2\left(x_1^2 + x_2^2\right)\right] \text{ and } \nabla g_m = \nabla^2\left[\overline{v}_m + (1/2)\omega^2\left(x_1^2 + x_2^2\right)\right]$$

   g) Compute the surface increment $\dot{\varphi}_m$ by

$$\dot{\varphi}_m = \left(\nabla g_m \circ \varphi_m\right)^{-1}\left(\dot{\widetilde{G}}_m - \nabla u_m \circ \varphi_m\right)$$

   and update surface map by $\varphi_{m+1} = \varphi_m + \Delta_m \dot{\varphi}_m$

   h) Update direction vector and gravity vector by

$$h_{m+1} = \left\{\left[-\left(\nabla g_m\right)^{-1} g_m\right] \circ \varphi_m\right\} \circ \left(\varphi_{m+1}\right)^{-1}, \quad G_{m+1} = g_m \circ \varphi_m$$

   i) Stop if $\left\|g_m \circ \varphi_m - G\right\| + \left\|\overline{v}_m \circ \varphi_m - W\right\| < tol$ for given tolerance *tol*, $\|\cdot\|$ usually chosen to be an $\mathcal{H}^a$-norm.

In *Costea et al. (2013)* the following convergence result for the Nash-Hörmander iteration (Algoritm 1) is proved, where it is assumed that the starting values W_0 and G_0 are already in a small neighborhood (in the Hölder space $C^{\alpha+\varepsilon}$) of the final values W and G.

Theorem 1. For $\alpha > 2 + 2\varepsilon$, $0 < a < \alpha$ and $\tau > 0$ small, such that $a - \alpha - \tau < 0$ there exist constants $\theta_0 > 0$, $C_\tau > 0$ subject to φ_m satisfy for all $m \geq 0$

$$\left\|\varphi - \varphi_m\right\|_{C^{\alpha+\varepsilon}} \leq C_\tau \left(\left\|W - W_0\right\|_{C^{\alpha+\varepsilon}} + \left\|G - G_0\right\|_{C^{\alpha+\varepsilon}}\right)\theta_m^{a-\alpha+\tau} .$$

3. BOUNDARY ELEMENT PROCEDURE

Inserting a single layer potential ansatz

$$u(x) = V\mu(x) = -\frac{1}{4\pi}\int_{\varphi_m\left(S^2\right)} \frac{\mu(y)}{|x-y|}\, ds_y \tag{10}$$

into the linearized Molodensky problem (Eq. (2)) translates the oblique Robin boundary condition to a second kind integral equation for the density μ on the surface $\varphi\left(\mathbb{S}^2\right)$, namely

$$B\mu(x) := \frac{1}{2}\cos\beta\mu(x) + K'(\boldsymbol{h})\mu(x) + V\mu(x) = f(x), \tag{11}$$

where $\beta = \measuredangle(\boldsymbol{n}, \boldsymbol{h})$, $K'(\boldsymbol{h}) = h \cdot \nabla V$ and $f = F(G, W) - \sum_{j=1}^{3} a_j A_j$.

The following variational formulation of the above integral equation is solved by boundary elements (BE): Find $\left(\mu_{m,h}, a_{j,m}^h\right) \in S_{h,m} \times \mathbb{R}^3$ subject to

$$\begin{gathered}\left\langle B\mu_{m,h}, \psi_h \right\rangle_{\varphi_m^h\left(\mathbb{S}^2\right)} + \sum_{j=1}^{3} \left\langle B a_{j,m}^h A_j, \psi_h \right\rangle_{\varphi_m^h\left(\mathbb{S}^2\right)} = \left\langle F_m^h, \psi_h \right\rangle_{\varphi_m^h\left(\mathbb{S}^2\right)} \quad \forall\, \psi_h \in S_{h,m}\,, \\ \left\langle \mu_{m,h}, A_k \right\rangle_{\varphi_m^h\left(\mathbb{S}^2\right)} = 0\,,\end{gathered} \tag{12}$$

where $S_{h,m}$ denotes the set of piecewise quadratic continuous functions on the approximate surface $\varphi_m^h\left(\mathbb{S}^2\right)$ and F_m^h is the projection of F_m onto $\varphi_m^h\left(\mathbb{S}^2\right)$. This surface is obtained starting from an initial regular mesh of plane triangles. Numerical experiments described below show that for p.w. quadratic polynomials the Hessian can be computed sufficiently accurately. The auxiliary exterior Dirichlet problem (Eq. (6)) is again solved by the boundary element method (BEM) with a single layer potential ansatz:

Find $\left(\tilde{\mu}_{m,h}, \tilde{a}_{j,m}^h\right) \in S_{h,m} \times \mathbb{R}^3$ subject to

$$\begin{aligned} \left\langle V\tilde{\mu}_{m,h}\,,\,\xi_h \right\rangle_{\varphi_m^h\left(\mathbb{S}^2\right)} + \sum_{j=1}^{3} \tilde{a}_{j,m}^h \left\langle VA_j\,,\,\xi_h \right\rangle_{\varphi_m^h\left(\mathbb{S}^2\right)} &= \left\langle w_m^h\,,\,\xi_h \right\rangle_{\varphi_m^h\left(\mathbb{S}^2\right)} \quad \forall\, \psi_h \in S_{h,m}\,, \\ \left\langle \tilde{\mu}_{m,h}\,,\,\tilde{A}_k \right\rangle_{\varphi_m^h\left(\mathbb{S}^2\right)} &= 0\,, \quad k = 1,\,2,\,3\,, \end{aligned} \tag{13}$$

where w_m^h is the projection of w_m on $\varphi_m^h\left(\mathbb{S}^2\right)$. The convergence as $h \to 0$ of the boundary element approximations $\left(\mu_{m,h}\,,\,a_{j,m}^h\right)$ and $\left(\tilde{\mu}_{m,h}\,,\,\tilde{a}_{j,m}^h\right)$ is shown in *Klees et al. (2001)*.

The crucial point for the numerical computation of the updates in the Nash-Hörmander algorithm is the Hessian $\nabla^2 \overline{v}_m$ on the surface $\varphi_m^h\left(\mathbb{S}^2\right)$, which must be approximated very accurately. This is difficult as the single layer potential ansatz for $\overline{v}_m$ leads to the evaluation of hypersingular integrals

$$\nabla^2 \overline{v}_m = -\frac{1}{4\pi}\, p.f. \int\limits_{\varphi_m\left(\mathbb{S}^2\right)} \nabla_x^2 \frac{1}{|x-y|}\, \overline{\mu}_m\left(y\right) ds_y\,, \qquad x \in \varphi_m\left(\mathbb{S}^2\right).$$

Since the gradient $g = \nabla \overline{v} = \nabla V \overline{\mu}_m$ can be computed analytically on plane surface pieces (see *Maischak, 2001a*), we approximate the second derivative of $\overline{v}$ by appropriate finite differences (FD). For the normal and tangential derivative of g we take

$$\frac{\partial\, g\left(x\right)}{\partial\, n} = \frac{4g\left(x+\delta\cdot n\right) - 3g\left(x\right) - g\left(x+2\delta\cdot n\right)}{2\delta}\,,$$

$$\frac{\partial\, g\left(x\right)}{\partial\, t} = \frac{g\left(x+\delta\cdot t\right) - g\left(x-2\delta\cdot n\right)}{2\delta} + O\left(\delta^2\right),$$

with stepsize δ. Second and higher{order derivatives have also been analyzed by *Schulz et al. (1998)* and *Schwab and Wendland (1999)*. They compute the second normal derivative from the less singular tangential derivatives using geometrically graded meshes near the singularity. For the current problem, a simpler approach gives sufficient accuracy.

In the computations, the step size δ is set to 10^{-4} for the normal component and to 10^{-5} for the tangential component when approximating second derivatives. For the presented numerical experiments the FD-approximation error is of magnitude 10^{-7} if no Galerkin-BEM approximation error were to occur. However, for very small step sizes the finite differences become numerically unstable, and for the given BE-spaces the BEM-error dominates the FD-error. If $H = \left(H_{ij}\right)$ denotes the exact and $H_h = \left(H_{h,ij}\right)$ the approximated Hessian, we measure the error in a point x as

$$\left[\sum_{i,j}\left(H_{h,ij}\left(x\right) - H_{ij}\left(x\right)\right)^2\right]^{1/2}.$$

Example 1. Let $\Omega = \left[-1/2, 1/2\right]^2$ be the domain and $u = \ln\|x\|$ the exact solution. Then the exact Hessian is

$$H(x) = \frac{1}{x^2}\begin{pmatrix} 1-2x_1^2 & -2x_1x_2 \\ -2x_1x_2 & 1-2x_2^2 \end{pmatrix}.$$

Figure 1 shows the pointwise error of the Hessian approximation in the point $x = (1/2, 1/3)$ for h-versions of BEM with polynomial degree $p = 0, 1, 2, 3$, as well as for a p-version with $h = 0.2$ versus the degrees of freedoms (DOF).

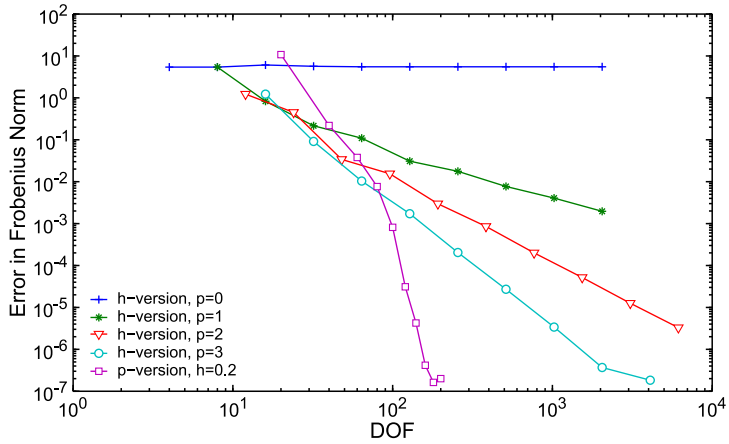

Fig. 1. Error of the Hessian approximation in 2D for a point on the boundary surface for variable degrees of freedom (DOF).

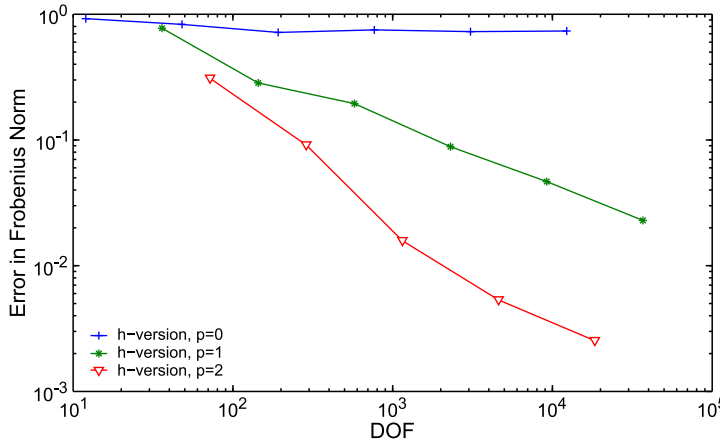

Fig. 2. The same as in Fig. 1, but in 3D.

Example 2. Let $\Omega = [-1,1]^3$ be the domain and g corresponding to the exact solution $u(x) = 1/\|x\|$ with Hessian

$$H(x) = \frac{3}{\|x\|^5}\begin{pmatrix} x_1^2 & x_1x_2 & x_1x_3 \\ x_1x_2 & x_2^2 & x_2x_3 \\ x_1x_3 & x_2x_3 & x_3^2 \end{pmatrix} - \frac{1}{\|x\|^3} I .$$

Figure 2 shows the error of the Hessian in $x = (1, 1/3, 1/3)$. For $p \geq 2$ we observe good convergence of the Hessian approximation.

4. NUMERICAL EXPERIMENTS

For the numerical experiments we set $\varphi : \mathbb{S}^2 \to \mathbb{R}^3$ to be $\varphi(x) = 1.1x$ and $\omega = 0$. This means that the sought surface is a sphere of radius 1.1 with gravity potential $W_{meas} = 1/1.1$ and gravity vector $G_{meas} = -\left(1/1.1^2\right)\left(x/|x|\right)$, both defined on $\mathbb{S}^2$. The initial approximation φ_0 is the unit sphere $\mathbb{S}^2$. Therefore, $W_0 = 1$, $G_0 = -x/|x|$ and $h_0 = x/2$.

The sphere $\mathbb{S}^2$ is approximated by a regular, quasi-uniform mesh consisting of triangles such that the nodes of each triangle lie on $\mathbb{S}^2$. More precisely, the mesh defines an icosahedron which is generated by maiprogs (*Maischak, 2001b*). This mesh yields a domain approximation error and is kept fixed for the entire Nash-Hörmander algorithm. The main advantage is that only the coordinates of the nodes have to be updated and not the entire mesh itself. This corresponds to a continuous, piecewise linear representation of φ_m, the new surface at the m-th update of the algorithm.

The polynomial degree on each triangle is $p = 2$, and h_m in Eq. (3) is represented by a discontinuous piecewise constant function via interpolation in the midpoints of each triangle. Furthermore, G_m is the linear interpolation in the nodes of the BEM approximation of $g|_{\varphi_m(\mathbb{S}^2)}$, obtained via $\overline{v}_m$ from Eq. (6). Since hm and the normal on each triangle $\mathcal{T}_n$ are piecewise constant, the jump contributions can be easily computed analytically. Also, the operator $\mathcal{K}'(h)$ in Eq. (11) can be computed semi-analytically by computing the action of the dual operator $\mathcal{K}(h)$ on the test functions analytically (*Maischak, 2001a*) and performing an hp-composite Gaussian quadrature (*Schwab, 1994*) for the outer integration.

Since the boundary element space is the same for both the linear Molodensky problem (Eq. (2)) and the auxiliary Dirichlet problem (Eq. (6)), the same single layer potential matrix is used in both Eqs (12) and (13). However, the computation of the right hand side wm for the Dirichlet problem is very CPU time consuming if a direct computation by

means of Eq. (10) is used. Since the ansatz and test functions live on varying surfaces, the computation of one summand in Eq. (10) is as expensive as a semi-analytic computation of a single layer potential matrix. In particular, the computational time for the right hand side increases linearly with the number of iterations.

Since φ_m is piecewise linear, the Gauss quadrature nodes x for the outer integration are always mapped to exactly the same point on $\varphi_i\left(\mathbb{S}^2\right)$ under the mapping $\varphi_i \circ \varphi_m^{-1}(x)$ for each iteration step m. Therefore, if enough memory is available, $V_i \mu_i\left(\varphi_i \circ \varphi_m^{-1}(x)\right)$ needs only be computed once and is stored for all the following iterations, keeping the computational time for the right-hand side of Eq. (13) constant for all iterations m. This optimization together with the following parallelization of the code leads to a tremendous reduction of computing time.

With the solution of the Dirichlet problem (Eq. (13)) at hand, the update of the surface in the nodes can be performed as defined in Eq. (4) and with g, ∇g computed as in Section 3. The computation of one iteration is very CPU time consuming and therefore, parallelization of the code is crucial. Without parallelization and optimization of the code we need $4 + 2m$ hours for the m-th iteration. However, with parallelization and optimization we need only 20 minutes for each of the m iterations for $N = 2$ -icosahedron refinements corresponding to 320 triangles, whereas we need 3 hours for each of the m iterations for $N = 3$ -icosahedron refinements corresponding to 1280 triangles. The numerical experiments were carried out on a cluster with 5 nodes à 8 cores with 2.93 Ghz and 48 GB memory, where each core uses two Intel Nehalem X5570 processors.

In the following three different numerical experiments are presented. The first and the second experiment use the classical Nash-Hörmander algorithm with and without smoother as described in Section 2. For the third experiment, the following restarted algorithm with smoother is used.

Algorithm 2. (Nash-Hörmander algorithm with restart)

1. For given measured data W, G and $k \in \mathbb{R}$, choose W_0, G_0, h_0, φ_0, $\theta_0 \gg\sim 1$, $\kappa \gg 1$
2. Compute W_k, G_k, φ_k in Algorithm 1
3. Stop if $\left\| \left| G_k - G \right| \right\| + \left\| \left| W_k - W \right| \right\| < tol$
4. Else set $W_0 = W_k$, $G_0 = G_k$, $h_0 = h_k$, $\varphi_0 = \varphi_k$, choose κ, θ_0, and go to 2.

Since the sought surface is also a sphere, we can expect that the sequences of computed surfaces are slightly perturbed spheres as well. The perturbation should be a direct result of the domain approximation, different discretization errors and rounding errors. Fig. 3 displays the mean l_2 error of the radius defined as

$$\left\| e_r \right\| = \frac{1}{N}\left[\sum_{i=1}^{N} \left(\left\| \mathrm{node}(i) \right\|_2 - 1.1 \right)^2 \right]^{1/2}$$

where N is number of nodes, versus the number of iterations of Algorithm 1. Whereas the algorithm itself takes care of the linearization error introduced by the linearization of the

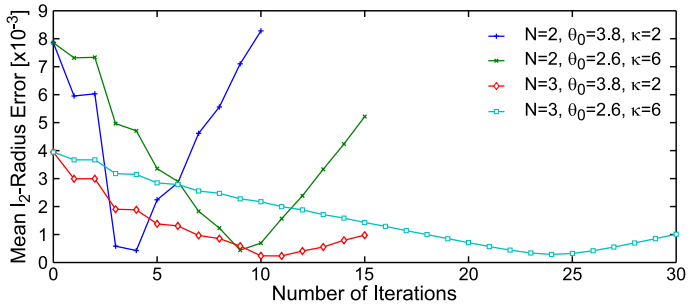

Fig. 3. Mean Radius-Error in the l_2-norm with smoother.

Molodensky problem, the algorithm does not treat the propagation of the discretization errors. Therefore, from a certain iteration step onwards the propagation of the spatial discretization error, for solving the linearized Molodensky problem, the auxiliary Dirichlet problem and computing the Hessian approximately, becomes dominating. Refining the mesh reduces the error and yields only a mild increase of the error for large iteration numbers. However, this is a topic of further research.

We have performed several numerical experiments with different parameters θ_0 and κ. Firstly, if the amount of data smoothing is too small, the algorithm is unstable as expected. Secondly, if the amount of data smoothing is too large, then the essential information in the right hand side in the linearized Molodensky problem is lost in the first steps and in combination with the numerical errors convergence is lost. Also if the amount of smoothing does not decay sufficiently fast, the right hand side in the linearized Molodensky problem is close to machine precision leading to an ill-conditioned Hessian.

Here, we shortly comment how to perform smoothing with the heat kernel as it is used in the above example. To smooth an arbitrary function F, the heat equation with the Laplace-Beltrami operator on the respective surface is solved, where F is the initial data.

$$\frac{\partial}{\partial t}u(x,t)-\Delta u(x,t)=0 \quad \text{in } \varphi_m\left(\mathbb{S}^2\right)\times(0,\infty),$$

$$(x,0)=F(x) \quad \text{in } \varphi_m\left(\mathbb{S}^2\right).$$

The unique solution of this problem is given by

$$u(x,t)=\sum_{j=0}^{\infty} \mathrm{e}^{-\lambda_j t}\left\langle F,\psi_j\right\rangle\psi_j(x). \tag{14}$$

At $t = 0$ we have

$$u(x,0)=\sum_{j=}^{\infty}\beta_j\psi_j(x)=F(x),$$

where β_j are the Fourier coefficients $\left\langle F, \psi_j \right\rangle$. Here $0 = \lambda_0 < \lambda_1 \leq \lambda_2 \leq \ldots$ are the eigenvalues and ψ_0, ψ_1, ψ_2, … the corresponding eigenfunctions for the Laplace-Beltrami operator Δ, i.e. there holds

$$\Delta \psi_j = -\lambda_j \psi_j . \tag{15}$$

The eigenfunctions ψ_j form an orthonormal basis in $\mathrm{L}^2\left(\varphi\left(\mathbb{S}^2\right)\right)$.

Having the discretized surface, Eq. (15) can be solved approximately using the FEM method with continuous piecewise linear polynomials leading to the generalized eigenvalue problem with the stiffness matrix C and the mass matrix A of the Laplace-Beltrami operator Δ

$$C\psi_h = \lambda_h A \psi_h , \tag{16}$$

where ψ_h denotes the unknown L^2-orthonormal eigenfunction, evaluated at the mesh vertices. With ψ_h solving Eq. (16)

$$\mathrm{e}^{-t\Delta} F(x) = \sum_{j=0}^{M} \mathrm{e}^{-t\lambda_{j,h}} \left\langle F, \psi_{j,h} \right\rangle \psi_{j,h}(x),$$

where M must be sufficiently large. Once we obtained the components $\psi_{j,h}$ of the eigenfunctions ψ_h, we compute the Fourier coefficients $\beta_{j,h}$ as presented in (*Seo et al., 2010, Eq. (10)*). Therewith,

$$u_h(x,t) = \sum_{j=0}^{M} \mathrm{e}^{-\lambda_{j,h} t} \beta_{j,h} \psi_{j,h}(x). \tag{17}$$

For a different filtering approach see *Čunderlík et al. (2013)*. For our numerical experiments F is always of the structure $G_{meas} - G_m + \sum_{j=0}^{m-1} \Delta_j \dot{\tilde{G}}_j$ (see Eq. (9)). We use $u_h\left(x, 1/\theta_m^2\right)$, where $t = 1/\theta_m^2$ in Eq. (17) as the smoothed F, where θ_m is computed by Eq. (7).

Figure 4 displays the mean l_2 error of the radius versus the number of restarts for the restarted algorithm with the above given smoothing operator. In the extreme case, in which the algorithm is restarted after each iteration, we still observe the same structural behavior as for the other experiments. In particular, from the third restart onwards the discretization error propagation becomes dominating again. Again the error can be reduced by refining the mesh.

Table 1 shows the pointwise error

$$\left|u_N(\boldsymbol{q}) - u(\boldsymbol{q})\right| := \sqrt{\frac{1}{10242}} \left(\sum_{i=1}^{10242} \left|u_N(\boldsymbol{q}_i) - u(\boldsymbol{q}_i)\right|^2 \right)^{1/2}$$

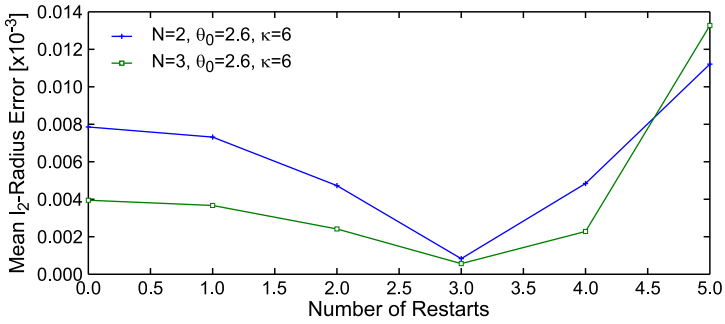

Fig. 4. Mean radius-error in the l_2-norm with smoother and restart.

Table 1. Pointwise errors $\left|u_N(\boldsymbol{q})-u(\boldsymbol{q})\right|$ for the linearized Molodensky problem with smoother. DOF: degrees of freedom, EOC: experimental order of convergence

Iteration	DOF	$\left\|u_N(\boldsymbol{q})-u(\boldsymbol{q})\right\|$	EOC
0	120	1.02926e+01	
	480	3.89526e-00	0.70
	1920	1.03431e-00	0.96
	7680	2.74648e-01	0.96
1	120	5.75594e+01	
	480	3.62558e-00	1.99
	1920	1.047666e-00	0.90
	7680	3.02160e-01	0.90
2	120	2.93091e+01	
	480	1.00035e+01	0.77
	1920	2.69169e-00	0.95
	7680	7.24262e-01	0.95

computed in a set of 10242 exterior points for the linearized Molodensky problem with smoother ($\theta_0 = 2.6$, $\kappa = 6$) for the first three Nash-Hörmander iterations (*Klees et al.,2001*). Here $u(\boldsymbol{q})$ is obtained by extrapolation. For all three iterations we obtain similar experimental order of convergence (EOC) with respect to the degrees of freedom (DOF) in space. Due to the domain approximation by plane triangles, the EOC is bounded.

Figure 5 displays the sequence of obtained spheres.

For large scale applications one has to use standard reduction methods for BEM to reduce the computational complexity, e.g. *H*-matrices and/or multipole expansion or wavelet compression techniques. All these techniques can be applied to speed up our algorithm and allow computations on finer meshes.

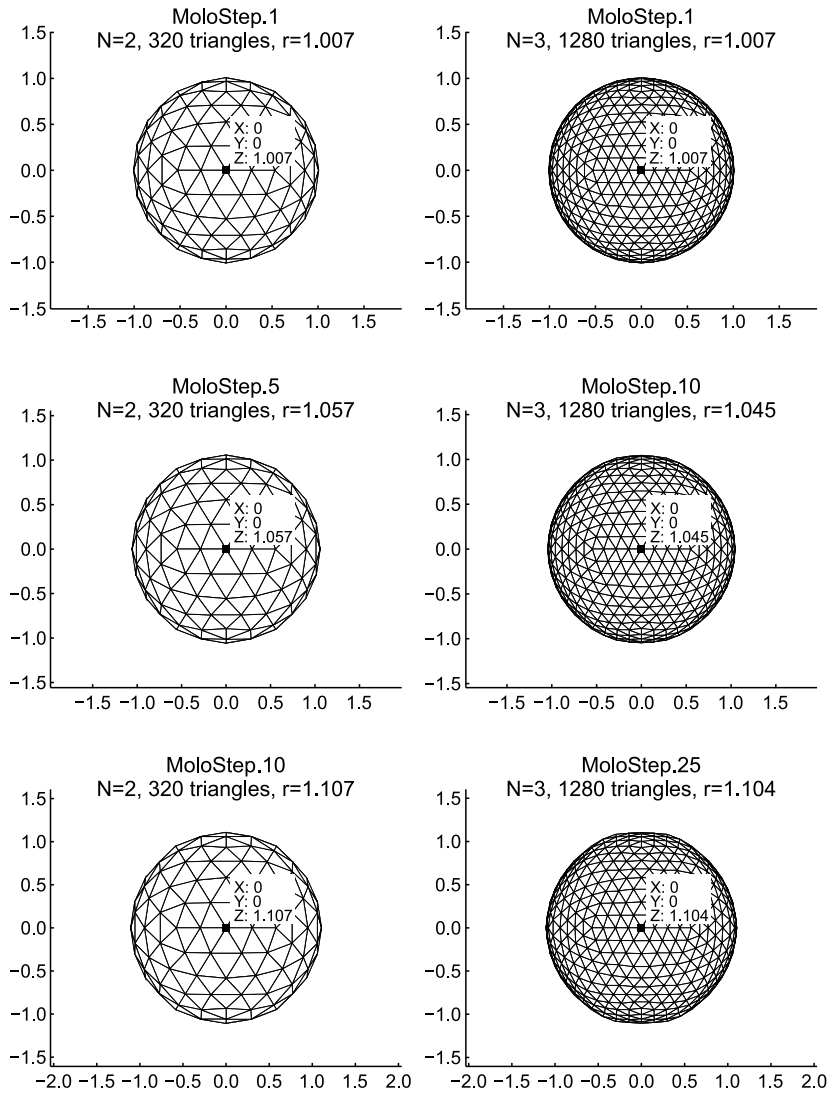

Fig. 5. Sequence of spheres obtained by Algorithm 1. $N = 2$ and $N = 3$ icosahedron refinements with smoother, $\theta_0 = 2.6$; $\kappa = 6$.

5. CONCLUSIONS

To solve the nonlinear Molodensky problem, a free boundary problem, we iteratively compute a sequence of approximate solutions. More precisely, this sequence is the solution of a sequence of linearized problems. In order to overcome the well known loss of regularity through out the iterations we apply a smoothing technique. Altogether, we

have shown that the rigorous numerical solution of the nonlinear Molodensky problem is computational feasible. For efficient, black-box type application to realistic geodetic data, the stability and accuracy of the discrete version need improvements by further developments with focus on domain discretization.

Acknowledgments: This work was supported by the cluster of excellence QUEST, the Danish National Research Foundation (DNRF) through the Centre for Symmetry and Deformation and the Danish Science Foundation (FNU) through research grant 10-082866.

References

Ardalan A.A. and Grafarend E.W., 2001. Somigliani-Pizzetti gravity: The international gravity formula accurate to the sub-nanoGal level. *J. Geodesy*, **75**, 424–437.

Costea A., Gimperlein H. and Stephan E., 2013. A Nash-Hörmander iteration and boundary elements for the Molodensky problem. *Numer. Math.*, DOI: 10.1007/s00211-013-0579-8 (in print).

Čunderlík R. and Mikula K., 2010. Direct BEM for high-resolution global gravity field modelling. *Stud. Geophys. Geod.*, **54**, 219–238.

Čunderlík R., Mikula K. and Mojzeš M., 2008. Numerical solution of the linearized fixed gravimetric boundary-value problem. *J. Geodesy*, **82**, 15–29.

Čunderlík R., Mikula K. and Tunega M., 2013. Nonlinear diffusion filtering of data on the earths surface. *J. Geodesy*, **87**, 143–160.

Fasshauer G. and Jerome J.W., 1999. Multistep approximation algorithms: Improved convergence rates through postconditioning with smoothing kernels. *Adv. Comput. Math.*, **10**, 1–27, DOI: 10.1023/A:1018962112170.

Freeden W. and Mayer C., 2006. Multiscale solution for the Molodensky problem on regular telluroidal surfaces. *Acta Geod. Geophys. Hungarica*, **41**, 55–86.

Heck B., 2002. Integral equation methods in physical geodesy. In: Grafarend E.W., Krumm F.W. and SchwarzeV.S. (Eds.), *Geodesy - The Challenge of the 3rd Millenium*. Springer-Verlag, Heidelberg, Germany, 197–206.

Heiskanen W.A. and Moritz H., 1993. *Physical Geodesy*. W.H. Freeman, San Francisco, CA.

Holota P., 1997. Coerciveness of the linear gravimetric boundary problem and a geometrical interpretation. *J. Geodesy*, **71**, 640–651.

Hörmander L., 1976. The boundary problems of physical geodesy. *Arch. Rational Mech. Anal.*, **62**, 1–52.

Jerome J.W., 1985. An adaptive Newton algorithm based on numerical inversion: regularization as postconditioner. *Numer. Math.*, **47**, 123–138.

Klees R., van Gelderen M., Lage C. and Schwab C., 2001. Fast numerical solution of the linearized Molodensky problem. *J. Geodesy*, **75**, 349–362, DOI: 10.1007/s001900100183.

Maischak M., 2001a. *Analytical Evaluation of Potentials and Computation of Galerkin Integrals on Triangles and Parallelograms*. Technical Report, ifam50 (http://www.ifam.uni-hannover.de/~maiprogs/).

Maischak M., 2001b. *Technical Manual of the Program System maiprogs* (http://www.ifam.uni-hannover.de/~maiprogs/).

Molodensky M., 1958. *Grundbegriffe der geodätischen Gravimetrie*. VEB Verlag Technik, Berlin, Germany (in German).

Molodensky M.S., Yeremeev V.F. and Yurkina M.I., 1960. Methods for study of the external gravitational field and figure of the Earth. *TRUDY TsNIIGAiK*, **131**, Geodezizdat, Moscow, Russia (English translat.: Israel Program for Scientific Translation, Jerusalem 1962).

Moser J., 1966a. A rapidly convergent iteration method and nonlinear differential equations - I. *Ann. Scuola Norm. Sup. Pisa*, **20**, 265–315.

Moser J., 1966b. A rapidly convergent iteration method and nonlinear differential equations - II. *Ann. Scuola Norm. Sup. Pisa*, **20**, 499–535.

Nash J., 1960. The embedding problem for Riemannian manifolds. *Ann. Math.*, **63**, 20–23.

Schulz H., Schwab C. and Wendland W.L., 1998. The computation of potentials near and on the boundary by an extraction technique for boundary element methods. *Comput. Meth. Appl. Mech. Eng.*, **157**, 225–238.

Schwab C., 1994. Variable order composite quadrature of singular and nearly singular integrals. *Computing*, **53**, 173–194.

Schwab C. and Wendland W.L., 1999. On the extraction technique in boundary integral equations. *Math. Comp.*, **68**, 91–122.

Seo S., Chung M.K. and Vorperian H.K., 2010. Heat kernel smoothing using Laplace-Beltrami eigenfunctions. In: Jiang T., Navab N., Pluim J.P.W. and Viergever M.A. (Eds.), *Medical Image Computing and Computer-Assisted Intervention - MICCAI 2010*: *Part III*. Lecture Notes in Computer Science **6363**, Springer-Verlag, Heidelerg, Germany, 505–512.